INVESTIGATION OF THE EFFECTS OF TEMPERATURE AND pH ON THE FORMATION OF METAL OXIDE NANOPHASE IN THE GRAPHENE/Fe_3O_4/CuO NANOCOMPOSITE COMBUSTION CATALYST SYSTEM SYNTHESIZED VIA SONOCHEMICAL TECHNIQUE

NGHIÊN CỨU ẢNH HƯỞNG CỦA NHIỆT ĐỘ VÀ pH ĐẾN SỰ HÌNH THÀNH PHA NANO OXIT KIM LOẠI TRONG HỆ XÚC TÁC CHÁY NANOCOMPOSITE GRAPHENE/Fe_3O_4/CuO TỔNG HỢP BẰNG PHƯƠNG PHÁP SIÊU ÂM

Vu Tien Cong[1,2,*], Nguyen Duc Long[2], Nguyen Thi Huong[1], Vu Minh Thanh[1]

DOI: http://doi.org/10.57001/huih5804.2025.193

ABSTRACT

This study investigates the synthesis process of Graphene/Fe_3O_4/CuO nanocomposite via the coprecipitation method assisted by ultrasonic waves. The effects of reaction temperature and pH on the formation of magnetic iron oxide (Fe_3O_4) and copper oxide (CuO) in the Graphene-based nanocomposite were examined using X-ray diffraction (XRD). The morphology, composition, and porosity of the synthesized Graphene/Fe_3O_4/CuO nanocomposite were characterized by scanning electron microscopy coupled with energy-dispersive X-ray spectroscopy (SEM-EDX) and Brunauer-Emmett-Teller (BET) surface area analysis. The synthesized samples were investigated with respect to variations in pH, reaction temperature, and NaOH addition rate. The optimized sample exhibited crystallite and particle sizes of Fe_3O_4 and CuO below 20nm, with a specific surface area of 71.1m^2/g and an average pore diameter of 2.9nm, indicating strong potential as a combustion catalyst for composite propellants.

Keywords: *Graphene/Fe_3O_4/CuO, nanocomposite, sonochemical, nanophase composition.*

TÓM TẮT

Bài báo này nghiên cứu khảo sát quá trình tổng hợp nanocomposite Graphene/Fe_3O_4/CuO bằng phương pháp đồng kết tủa dưới sự hỗ trợ của siêu âm. Ảnh hưởng của nhiệt độ phản ứng và pH của hệ lên sự hình thành pha oxit của nano oxit sắt từ và nano oxit CuO của hệ nanocomposite nền Graphene được nghiên cứu bằng phương pháp nhiễu xạ tia X. Hình thái học, thành phần, độ xốp của vật liệu nanocomposite Graphene/Fe_3O_4/CuO chế tạo được đánh giá đặc trưng bằng phương pháp kính hiển vi điện tử quét - tán xạ năng lương tia X (SEM-EDX), và phân tích diện tích bề mặt theo Brunaure-Emmet-Teller (BET). Các mẫu khảo sát sự phụ thuộc vào độ pH, nhiệt độ phản ứng và tốc độ cấp NaOH. Mẫu tối ưu cho kích thước tinh thể cũng như kích thước hạt của Fe_3O_4 và CuO nhỏ hơn 20nm, diện tích bề mặt 71,1m^2/g với kích thước mao quản trung bình 2,9nm cho tiềm năng tốt để làm xúc tác cháy cho thuốc phóng hỗn hợp.

Từ khóa: *Graphene/Fe_3O_4/CuO, nanocomposite, phương pháp siêu âm, thành phần pha oxit*

[1]Institute of chemistry and materials, Academy of Military Science and Technology, Vietnam
[2]Institute of Propellants and Explosives,Vietnam Defense Industry, Vietnam
[*]Email: congph40@gmail.com
Received: 20/02/2025
Revised: 22/5/2025
Accepted: 28/5/2025

1. INTRODUCTION

Among the various catalysts investigated, transition metal oxides especially iron and copper oxides have shown great promise in promoting the thermal decomposition of amoni perchlorat (AP). (AP) is widely used as the primary oxidizer, playing a decisive role in determining combustion performance and burn rate of composite propellants [1, 2] . However, AP typically exhibits a high decomposition temperature (~450°C), which limits the reaction rate and overall efficiency of the combustion process [3]. Consequently, the use of catalysts to lower the decomposition temperature of AP, reduce activation energy, and enhance the heat release of the decomposition reaction has become a pivotal research direction in the development of energetic materials [4, 5]. Their catalytic activity is attributed to their ability to provide active sites and accelerate redox reactions [4, 6, 7]. Studies have demonstrated that the addition of CuO can reduce the peak decomposition temperature of AP by approximately 73 -91°C, while significantly increasing the reaction heat and rate [8, 9]. Similarly, iron oxide nanoparticles, such as Fe_2O_3 [10] and Fe_3O_4 [11], can lower the decomposition temperature of AP by 50 - 71°C, thereby enhancing the combustion rate of composite solid propellants [12, 13].

Recently, graphene-based materials, including graphene oxide (GO) and reduced graphene oxide (rGO), have emerged as effective supports for addressing the critical challenge of nanoparticle agglomeration in metal oxide catalysts. These supports enable uniform dispersion of metal oxide nanoparticles and substantially improve catalytic efficiency compared to using metal oxides alone [14]. Graphene's two-dimensional structure, high surface area (2630m^2/g), and excellent thermal and electrical conductivity facilitate optimal interaction between catalysts and reactants, while preventing catalyst aggregation [2, 3]. Furthermore, the presence of oxygen-containing functional groups (hydroxyl, epoxy, carboxyl) on GO and rGO improves compatibility and enables strong anchoring of oxide nanoparticles through chemical and electrostatic interactions, making them favorable candidates for catalyst design [2, 3]. In contrast, pristine graphene has been less commonly employed due to its ideal sp^2-hybridized structure, which offers limited interaction with metal oxide nanoparticles primarily through van der Waals forces, hydrogen bonding, π–π stacking (if functionalized), or surface electrostatic interactions [15]. Nevertheless, in practice, graphene sheets invariably possess structural defects (e.g., carbon vacancies), and traces of oxygen-containing groups often remain due to fabrication processes. These features serve as potential active sites for interaction with metal oxides [16].

Recent experimental studies have confirmed the high catalytic efficiency of metal oxide catalysts supported on graphene. Notably, iron oxides have been extensively studied in AP decomposition systems. For instance, Fe_2O_3/rGO has been reported to reduce the AP decomposition temperature by up to 119°C [2], while Fe_2O_3 /graphene enhances the combustion rate of propellants by 52% (compared to 37% with Fe_2O_3 nanoparticles alone). Furthermore, surface-functionalized or encapsulated Fe_2O_4/graphene (e.g., Graphene-NH_2, Graphene-SO_3H) can double the combustion rate compared to systems without catalysts [17]. Likewise, the CuO/GO nanocomposite has demonstrated a 99°C reduction in the peak decomposition temperature of AP [2]. These findings underscore the potential of graphene-supported CuO and iron oxide nanocomposites, particularly the CuO/Fe_2O_4 hybrid, which may exhibit synergistic effects that enhance catalytic performance.

Several synthesis methods have been developed for graphene/metal oxide nanocomposites, including co-precipitation, sol-gel, hydrothermal, and solvothermal techniques [2, 3]. These methods allow precise control over particle size and morphology while ensuring uniform distribution across the graphene surface. Among them, co-precipitation stands out as the simplest method, requiring no complex equipment and allowing the use of ultrasonic probes to assist in reaction kinetics and achieve fine nanoparticle dispersion on graphene.

In this study, we present a detailed investigation into the ultrasonic-assisted co-precipitation synthesis of CuO/Fe_3O_4/graphene nanocomposites, focusing on the influence of synthesis parameters such as temperature, pH, and reaction rate. This method offers high efficiency and simplicity without requiring high-temperature calcination, distinguishing it from most previously reported approaches.

2. EXPERIMENT

2.1. Materials

Iron(II) chloride tetrahydrate ($FeCl_2{\cdot}4H_2O$, ≥ 99.9%), Iron(III) chloride hexahydrate ($FeCl_3.6H_2O$, ≥ 99.9%), Copper(II) chloride dihydrate ($CuCl_2{\cdot}2H_2O$, ≥ 99.9%),

Sodium hydroxide (NaOH, ≥ 99.5%), and Hydroxylamine hydrochloride ($NH_2OH{\cdot}HCl$, ≥ 98.0%), were all synthesis-grade chemicals purchased from Merck. Graphene (Gr), Nitrogen gas (N_2, ≥ 99.9%) and Ethanol (≥ 99.5%) was acquired from domestic companies in Vietnam.

2.2. Synthesis of CuO/Fe_3O_4/Graphene nanocomposites

Stock solutions of $FeCl_3$ (0.5M), $CuCl_2$ (0.5M), $FeCl_2$ (0.25M), NaOH (1M), and $NH_2OH{\cdot}HCl$ (0.1M) were prepared in advance. Notably, $FeCl_2$ (0.25M) solution was freshly prepared on the day of the experiment to ensure stability. A total of 0.1g of graphene powder was weighed into a beaker, followed by the addition of approximately 100mL of deionized water and two drops of ethanol to aid in wetting the material. Next, 3.5mL of each $FeCl_2$ and $FeCl_3$ solutions were added to the beaker, which was then placed in a temperature-controlled water bath at a preset temperature. An ultrasonic probe and a pH meter electrode were immersed into the solution, and nitrogen gas continuously blew over the surface at a rate of approximately 2mL/min to maintain an inert atmosphere then the ultrasonication was started. The NaOH solution was added dropwise under continuous pH monitoring until the target pH was reached. After 2 minutes, 5mL of $CuCl_2$ solution was added to the mixture, followed by continued addition of NaOH until the second predetermined pH value was achieved. Ultrasonic treatment was carried out until a total duration of 45 minutes was achieved.

The resulting suspension was allowed to stand undisturbed for 12 hours. The supernatant was then decanted, and the solid residue was collected by centrifugation. The washing and centrifugation steps were repeated 3 to 4 times with deionized water. In each washing cycle, 1 - 2 drops of $NH_2OH{\cdot}HCl$ solution were added to adjust the pH. When the pH of the wash solution reached the range of 6.5 - 7.5, a final rinse with ethanol was performed, followed by centrifugation. The final product was dried at 60°C for 12 hours.

2.3. Experimental Design and Sample codes

In this study, the effects of solution pH, reaction temperature, and NaOH addition rate were systematically investigated. The experimental conditions and corresponding sample codes are summarized in Table 1.

Table 1. Summary of Sample Codes and Investigated Parameters

pH Variation Study *(T = 70°C; NaOH addition rate = 4 mL/min)*	pH Value	9	10	11	12	13
	Sample Code	pH9	pH10	pH11	pH12	pH13
Temperature Variation Study *(pH = 12; NaOH addition rate = 4 mL/min)*	Temperature (°C)	30	50	70	85	
	Sample Code	T30	T50	T70	T85	
NaOH Addition Rate Study *(pH = 11; T = 70°C)*	Rate (mL/min)	0.5	2.0	4.0	6.0	
	Sample Code	V0.5	V2.0	V4.0	V6.0	

2.4. Characterization of Materials

The synthesized materials were characterized using X-ray diffraction (XRD) to identify their crystalline phases. Measurements were conducted on a D8 Advance diffractometer (Bruker) equipped with a monochromatic Cu Kα radiation source (λ = 1.5406Å), operating at 40mA and 40kV. The diffraction patterns were recorded over a 2θ range of 20° - 80° with a step size of 0.0297°. Crystallite size was calculated using both the Scherrer equation (1) and the Williamson-Hall method (2).

$$D = \frac{k.\lambda}{\beta \cos\theta} \quad (1)$$

$$\beta \cos\theta = \frac{k\lambda}{D} + 4\varepsilon \sin\theta \quad (2)$$

Where:

β: Full Width at Half Maximum (FWHM) of the diffraction peak (radians, instrument-corrected)

θ: Bragg angle (radians)

λ: X-ray wavelength (Cu Kα = 1.5406Å = 0.15406nm)

k: Shape factor (commonly taken as 0.9)

D: Average crystallite size (nm)

ε: Microstrain or lattice distortion (dimensionlesss)

BET surface area analysis was performed using a Tristar II 3030 Plus analyzer (G&G Instrument). Surface morphology and elemental distribution were examined using SEM and SEM-EDX mapping on a Hitachi S-4800 field emission scanning electron microscope.

3. RESULTS AND DISCUSSION

3.1. XRD results

Figure 1 presents the XRD patterns of the synthesized samples under various experimental conditions, along with the calculated crystallite sizes based on the Scherrer equation (Equation 1). The results confirm the formation of distinct crystalline phases corresponding to Fe_3O_4, CuO, and graphene, as evidenced by their characteristic diffraction peaks.

Graphene exhibits a sharp and intense peak at approximately 2θ ≈ 26.6°, corresponding to the (003) plane, and a minor peak at ~43.3°, associated with the (101) plane. Both Fe_3O_4 and CuO exhibit strong peaks at ~35.5°, which correspond to the (311) plane of Fe_3O_4 and the $(\bar{1}11)$ plane of CuO, respectively. Despite the overlapping at this angle, the presence of Fe_3O_4 is further confirmed by a distinct peak at ~62.8° (440), while CuO is identified by peaks at ~38.8° (111) and ~48.8° $(\bar{2}02)$.

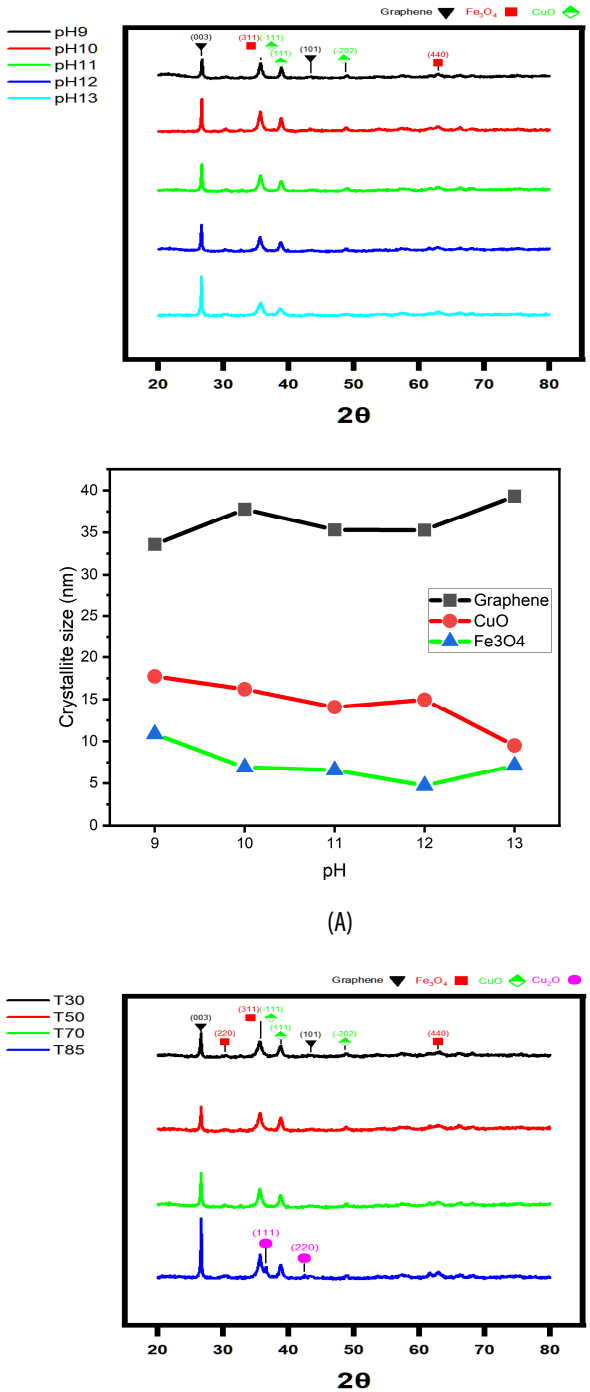

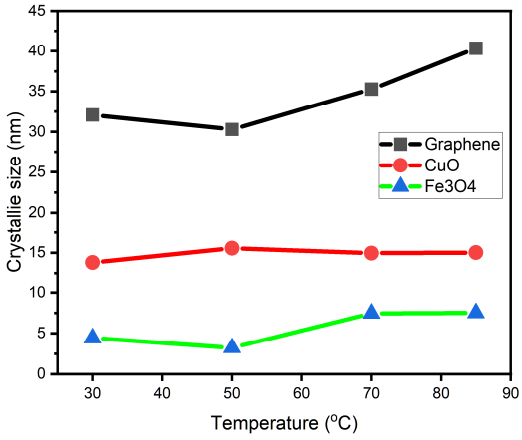

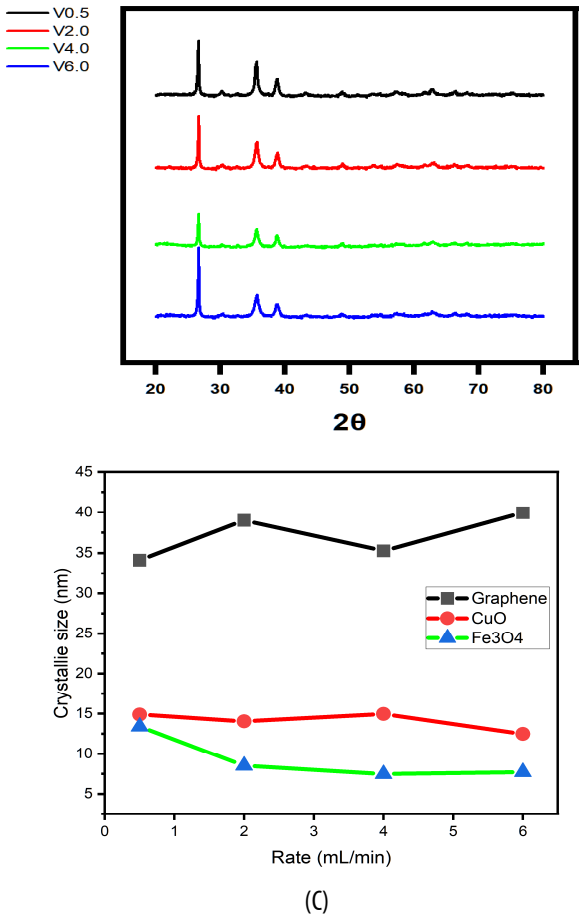

Figure 1. XRD patterns and corresponding crystallite sizes of individual components in the synthesized composites under varying experimental conditions: (A) environmental pH, (B) reaction temperature, and (C) NaOH addition rate

Additionally, broadening of peaks at higher diffraction angles is observed, which may partly result from instrumental effects. However, such broadening also suggests the presence of lattice defects within the composite structure. While the Scherrer equation does

not account for contributions from lattice strain or defects, the consistent use of synthesis method, sample components, and instrument across all measurements allows for a meaningful comparative analysis. Thus, crystallite sizes were estimated using the most prominent, non-overlapping peaks for each component: ~26.6° for graphene, ~62.8° for Fe_3O_4, and ~38.8° for CuO (the ~35.5° peak was excluded due to overlap between CuO and Fe_3O_4).

Although the Scherrer equation provides limited accuracy in estimating crystallite size for graphene, due to its inherently thin, layered morphology, it remains a valid tool for relative comparison when the samples are based on a similar matrix.

3.1.1. Effect of pH

The pH of the reaction medium has a significant impact on the formation of crystalline phases. At lower pH levels (pH 9 - 10), the characteristic peaks of Fe_3O_4 and CuO are sharper and exhibit higher relative intensities compared to those of graphene, indicating better crystallinity. This observation is consistent with the trend in crystallite sizes, which tend to be larger in the low-pH region than at higher pH levels.

Notably, the crystallite size of CuO decreases markedly with increasing pH, while that of Fe_2O_4 remains relatively stable in the range of approximately 4 - 7nm. This behavior may be attributed to the different reaction kinetics and stability of the two oxides. Fe_3O_4 appears to complete its crystallization during the ultrasonic treatment period, whereas CuO may continue to crystallize post-reaction. In low OH^- concentration environments, the slow growth of CuO crystals likely due to limited ion availability promotes the development of larger crystallites. Conversely, at higher OH^- concentrations, the rapid and complete reaction facilitates the formation of fully crystallized CuO with smaller crystallite sizes.

Table 2. Crystallite size (D) and microstrain (ε) of composites synthesized at different pH values, calculated using the Williamson-Hall method

pH	Fe_3O_4		CuO	
	D (nm)	ε	D (nm)	ε
9	16.51	0.6%	-72.98	124.5%
10	30.14	0.7%	44.73	0.4%
11	173.32	1.2%	15.76	0.1%
12	-12.49	1.9%	-51.35	124.6%
13	10.27	0.6%	20.39	0.2%

As previously mentioned, the broadening of characteristic peaks at higher diffraction angles is likely associated with the presence of crystallographic defects, which are quantitatively represented by microstrain (ε) in the Williamson-Hall equation (Equation 2). Table 2 presents the results of crystallite size and microstrain calculated using the Williamson-Hall method [18], Due to the lack of instrumental broadening data and the complex nature of the nanocomposite where distinct, isolated diffraction peaks are limited some calculated values for crystallite size (D), particularly for CuO and Fe_3O_4, appear abnormally high or even negative.

For the Fe_3O_4 phase, when ε exceeds 0.7%, the corresponding crystallite size becomes erratic, indicating the presence of significant internal lattice stress. The trend of increasing ε with higher pH suggests instability in crystal formation at elevated alkalinity. However, at pH 13, ε decreases again, possibly due to partial crystal disruption that relieves microstrain.

Regarding the CuO phase, the lowest microstrain (0.1%) was observed at pH 11, indicating relatively well-ordered microcrystals and yielding the smallest crystallite size. At pH 9 and 12, microstrain values were extremely high, which may point to lattice distortion or the formation of uncontrolled secondary phases.

In conclusion, a reaction pH in the range of 10 - 12 is optimal for synthesizing Fe_3O_4/CuO/graphene nanocomposites, striking a balance that favors the formation of stable nanocrystalline phases.

3.1.2. Effect of Reaction Temperature

As the reaction temperature increases, the intensity of the Fe_3O_4 diffraction peak at ~62.8° shows a noticeable enhancement, suggesting that Fe_3O_4 crystallizes more effectively at elevated temperatures. This is further supported by a significant increase in its calculated crystallite size from below 5 nm to over 7nm as the temperature rises to 70 - 85°C.

Interestingly, the CuO phase exhibits relatively stable crystallite sizes (approximately 15nm) and consistent peak intensities in the temperature range of 30 - 70°C, indicating thermal stability within this range. However, at 85°C, additional weak peaks appear at $2\theta \approx 36.5°$ and 42.4°, corresponding to the (111) and (220) planes of Cu_2O, respectively. This suggests that CuO may undergo partial reduction at higher temperatures. Such reduction could result from a combination of elevated ambient temperature and localized heating from the ultrasonic probe, which may induce the formation of Cu_2O as an

intermediate product en route to metallic copper, particularly at the nanoscale [19, 20]. Although the exact mechanism remains unclear and beyond the scope of this study, this observation highlights a potential thermal instability of CuO at high reaction temperatures, indicating that synthesis should be avoided at temperatures as high as 85°C.

For the graphene phase, both the intensity and sharpness of its characteristic peak increase significantly with temperature, leading to a notable rise in the calculated crystallite size. This trend may be attributed to the annealing effect of higher temperatures, which could reduce structural defects in the graphene lattice.

In summary, the optimal reaction temperature lies between 50°C and 70°C, which favors the formation of stable and balanced crystalline structures in the Fe_3O_4/CuO/graphene nanocomposite.

3.1.3. Effect of NaOH Addition Rate

The rate at which NaOH is added appears to have a relatively minor impact on the formation of crystalline phases. For the graphene phase, as previously discussed, variations in peak intensity and calculated crystallite size are likely attributed to sampling inconsistencies rather than synthesis conditions.

In the case of CuO, the crystallite size remains relatively stable, ranging from 12.5 to 14.9nm, with minimal variation across different NaOH addition rates. This indicates a good degree of crystallinity and resistance to kinetic changes during synthesis. Interestingly, for the Fe_3O_4 phase, a slower NaOH addition rate of 0.5mL/min leads to an increase in crystallite size. This may be explained by a gradual crystallization process under lower OH^- concentrations. At this rate, the reaction time required to fully form Fe_3O_4 is approximately four times longer than at 2.0mL/min, allowing more time for the growth of larger crystallites. Conversely, at a high addition rate of 6.0mL/min, pH control becomes more difficult, potentially disrupting the crystallization process. Therefore, an NaOH addition rate in the range of 2 - 4mL/min is considered optimal for achieving uniform and balanced crystallite growth.

Based on the above analyses, the Fe_3O_4/CuO/graphene nanocomposite synthesized at pH 11, 70°C, and a NaOH addition rate of 4mL/min is selected as the optimal sample for further investigation.

3.2. SEM and SEM–EDX Results

The surface morphology of the optimized sample was examined using scanning electron microscopy (SEM), as shown in Figure 2, and the elemental distribution was analyzed via EDX mapping.

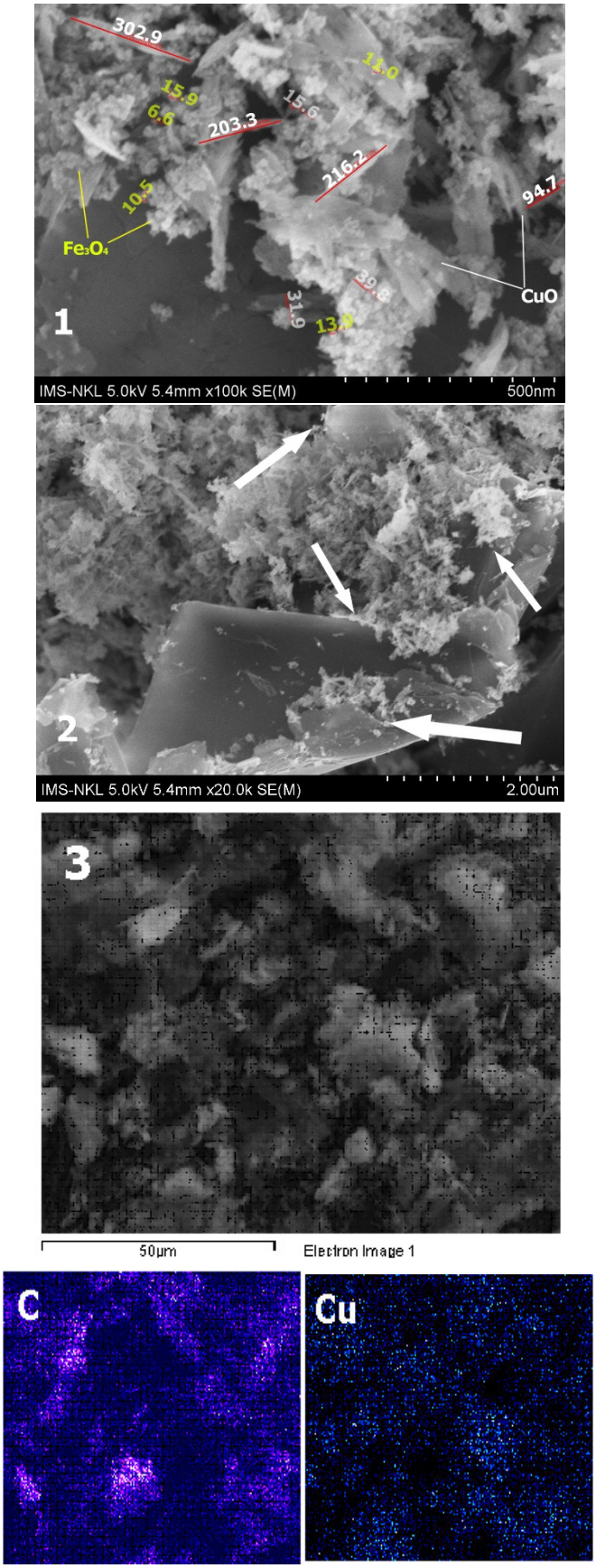

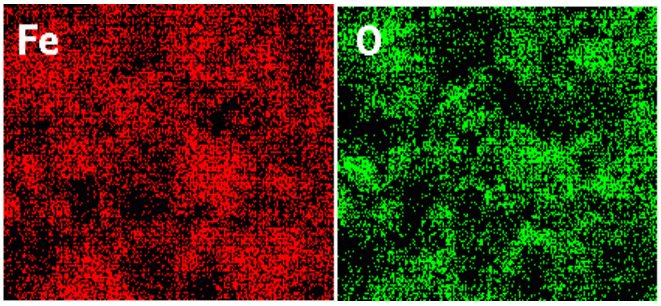

Figure 2. SEM images (1-2) show surface morphology and EDX mapping (3) shows the elemental distribution of the optimized sample

In Figure 2(1), CuO exhibits an elongated, needle-like morphology characteristic of monoclinic structures with rhomboidal needle-like geometry. These nanorods predominantly range from 100 - 200nm in length and 15 - 25nm in width, indicating preferential growth along the axial direction [21]. In contrast, Fe_3O_4, which crystallizes in a face-centered cubic (FCC) structure, appears as spherical nanoparticles with diameters ranging from 6 - 15nm.

Although Fe_3O_4 is magnetic, the particles remain relatively dispersed, with voids observed between them. This is likely due to the intercalation of CuO nanocrystals, contributing to a porous microstructure an advantageous feature for catalytic applications.

In Figure 2(2), nanoparticles can be observed scattered across the surface, particularly adhering to the edges of graphene sheets, as indicated by the arrows. EDX mapping reveals a relatively homogeneous distribution of Fe, Cu, and O throughout the imaged region, with Fe displaying notably uniform coverage. These oxides are primarily located in the voids between graphene sheets (visible as dark regions in the carbon map) and along the graphene edges. Additionally, Fe and Cu signals are detectable even on areas with high carbon intensity, indicating affinity and possible surface interactions between the oxides and the graphene matrix.

Table 3. Atomic percentages of elements from EDX spectra of the optimized sample

Element	Atomic %			Average	Theoretical value
C K	64.52	62.36	69.41		
O K	27.71	27.39	23.06		
Fe K	3.85	5.26	3.82		
Cu K	3.92	4.99	3.72		
n_{Fe}/n_{Cu}	0.982	1.054	1.027	1.021	1.050

EDX data on elemental composition (Table 3) further show that the Fe/Cu molar ratio of 1.021 closely matches the theoretical value of 1.050, suggesting high sample homogeneity and excellent synthesis efficiency. The elevated oxygen content is attributed to both metal oxide bonding and moisture adsorption during measurement. Furthermore, a small amount of surface oxygen is intrinsic to graphene, and discrepancies in light element quantification may also arise from the limited sensitivity of EDX toward low atomic number elements.

3.3. BET results

BET analysis of the optimized sample (pH 11) revealed a specific surface area of 71.1m^2/g. The adsorption isotherm corresponds to Type IV according to IUPAC classification, indicating that the sample predominantly contains mesopores (Figure 3). The isotherm exhibits a broad hysteresis loop over the relative pressure range of 0.4 to 0.95, suggesting a wide distribution of pore sizes. The sharp convergence of the adsorption and desorption branches at high relative pressure, along with the steep desorption curve, implies rapid desorption behavior characteristic of open-ended mesopores. The slightly stepped or kinked nature of the hysteresis loop further suggests a diversity of pore shapes rather than a uniform pore structure.

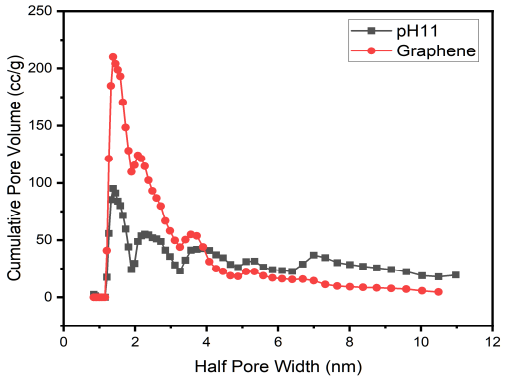

A

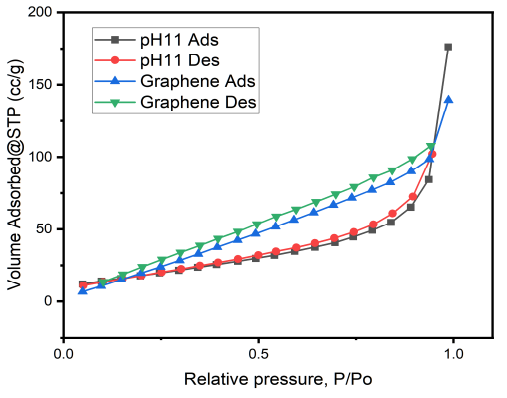

B

Figure 3. Comparison of DFT (A) and BET (B) data between the optimized sample (pH 11) and pristine graphene.

This observation is consistent with DFT (Density Functional Theory) analysis, which shows distinct dominant pore populations, particularly at 1.5nm, followed by peaks at approximately 2.5nm, 4.0nm, 5.3nm, and 7.5nm, with an average pore diameter of 2.9nm and a total pore volume of 0.1468 cm^3/g.

In comparison to pristine graphene (Figure 3), the incorporation of Fe_3O_4 and CuO oxides led to a significant reduction in pore volume at 1.5nm and 4.0nm, accompanied by an increase in the proportion of larger mesopores and an overall acceleration of nitrogen desorption (evident from the narrower gap between the adsorption and desorption curves relative to that of graphene). This behavior can be attributed to oxide nanocrystals occupying interlayer spaces between graphene sheets, forming secondary mesopores and partially blocking the native surface pores of graphene, thus reducing its specific surface area from 136m^2/g to 71.1m^2/g. These results corroborate findings from SEM and XRD analyses, indicating a random intermixing of oxide nanocrystals, as well as peak broadening at higher diffraction angles due to structural disorder.

4. CONCLUSION

The Fe_3O_4/CuO/graphene nanocomposite was thoroughly investigated, demonstrating clear dependencies on environmental pH, reaction temperature, and NaOH addition rate, with pH exerting the most significant influence. The optimal pH range for synthesis was determined to be 10 - 12. Reactions conducted at temperatures above 70°C are not recommended, and the ideal NaOH addition rate falls between 2 - 4mL/min. The Fe_3O_4/CuO/graphene nanocomposite exhibited a high degree of structural disorder, with notable microstrain within the crystalline lattice. The nanocrystals were observed to have lateral dimensions of 15 - 25nm for CuO and 6 - 15nm for Fe_3O_4, primarily distributed within the interlayer spaces and along the edges of graphene sheets. The random intermixing of CuO and Fe_3O_4 nanocrystals resulted in the formation of a diverse system of mesopores, with an average pore size of 2.9nm, providing a potential for heterogeneous catalytic applications.

REFERENCES

[1]. T. Chen, Y.W. Hu, C. Zhang, Z.J. Gao, "Recent progress on transition metal oxides and carbon-supported transition metal oxides as catalysts for thermal decomposition of ammonium perchlorate," *Defence Technology,* 17, 4, 1471-1485, 2021.

[2]. T. Zhang, et al., "Progress on the application of graphene-based composites toward energetic materials: A review," *Defence Technology,* 31, 95-116, 2024.

[3]. X. Fu, Y. Zhu, J. Li, L. Jiang, X. Zhao, X. Fan, "Preparation, characterization and application of nano-graphene-based energetic materials," *Nanomaterials,* 11, 9, 2374, 2021.

[4]. D. Li, et al., "Synthesis of covalently modified energetic graphene oxide/CuO composites with enhanced catalytic performance for thermal decomposition of ammonium perchlorate," *ACS omega,* 8, 25, 22876-22886, 2023.

[5]. S. Li, et al., "Preparation of different morphology Cu/GO nanocomposites and their catalytic performance for thermal decomposition of ammonium perchlorate," *RSC advances,* 12, 35, 22806-22814, 2022.

[6]. M. A. Fertassi, et al., "Catalytic effect of CuO nanoplates, a graphene (G)/CuO nanocomposite and an Al/G/CuO composite on the thermal decomposition of ammonium perchlorate," *Rsc Advances,* 6, 78, 74155-74161, 2013.

[7]. Q.L. Yan, F.Q. Zhao, K. K. Kuo, X.H. Zhang, S. Zeman, L. T. DeLuca, "Catalytic effects of nano additives on decomposition and combustion of RDX-, HMX-, and AP-based energetic compositions," *Progress in Energy and Combustion Science,* 57, 75-136, 2016.

[8]. S. G. Hosseini, Z. Khodadadipoor, M. Mahyari, "CuO nanoparticles supported on three-dimensional nitrogen-doped graphene as a promising catalyst for thermal decomposition of ammonium perchlorate," *Applied Organometallic Chemistry,* 32, 1, e3959, 2018.

[9]. P. L. Ríos, et al., "Novel in situ synthesis of copper nanoparticles supported on reduced graphene oxide and its application as a new catalyst for the decomposition of composite solid propellants," *RSC advances,* 9, 15, 8480-8489, 2019.

[10]. M. Zhang, F. Zhao, Y. Yang, J. Zhang, N. Li, H. Gao, "Effect of rGO–Fe_2O_3 nanocomposites fabricated in different solvents on the thermal decomposition properties of ammonium perchlorate," *CrystEngComm,* 20, 43, 7010-7019, 2018.

[11]. S. Zhiliang, T. Yulei, X. Yan, "Synthesis of Fe 3 O 4 nanowires and their catalytic activity towards thermal decomposition of ammonium perchlorate," *Russian Journal of General Chemistry,* 85, 926-929, 2015.

[12]. A. Dey, J. Athar, P. Varma, H. Prasant, A. K. Sikder, S. Chattopadhyay, "Graphene-iron oxide nanocomposite (GINC): an efficient catalyst for ammonium perchlorate (AP) decomposition and burn rate enhancer for AP based composite propellant," *Rsc Advances,* 5, 3, 1950-1960, 2015.

[13]. Y. Zhang, C. Meng, "Facile fabrication of Fe_3O_4 and Co_3O_4 microspheres and their influence on the thermal decomposition of ammonium perchlorate," *Journal of Alloys and Compounds,* 674, 259-265, 2016.

[14]. J. Liu, S. Chen, Y. Liu, B. Zhao, "Progress in preparation, characterization, surface functional modification of graphene oxide: A review," *Journal of Saudi Chemical Society,* 26, 6, 101560, 2022.

[15]. P. T. Yin, S. Shah, M. Chhowalla, K.B. Lee, "Design, synthesis, and characterization of graphene-nanoparticle hybrid materials for bioapplications," *Chemical reviews,* 115, 7, pp. 2483-2531, 2015.

[16]. B. Bukowski, N. A. Deskins, "The interactions between TiO_2 and graphene with surface inhomogeneity determined using density functional theory," *Physical Chemistry Chemical Physics,* 17, 44, 29734-29746, 2015.

[17]. S. Isert, L. Xin, J. Xie, S. Son, "The effect of decorated graphene addition on the burning rate of ammonium perchlorate composite propellants," *Combustion and Flame,* 183, 322-329, 2017.

[18]. G. Williamson, W. Hall, "X-ray line broadening from filed aluminium and wolfram," *Acta metallurgica,* 1, 1, 22-31, 1953.

[19]. J. Pike, S.W. Chan, F. Zhang, X. Wang, J. Hanson, "Formation of stable Cu2O from reduction of CuO nanoparticles," *Applied Catalysis A: General,* 303, 2, 273-277, 2006.

[20]. Y. Unutulmazsoy, C. Cancellieri, L. Lin, L. P. Jeurgens, "Reduction of thermally grown single-phase CuO and Cu_2O thin films by in-situ time-resolved XRD," *Applied Surface Science,* 588, 152896, 2022.

[21]. J. Zhu, et al., "Decorating graphene oxide with CuO nanoparticles in a water–isopropanol system," *Nanoscale,* 2, 6, 988-994, 2010.

THÔNG TIN TÁC GIẢ

Vũ Tiến Công[1,2], Nguyễn Đức Long[2], Nguyễn Thị Hương[1], Vũ Minh Thành[1]

[1]Viện Hoá học Vật liệu, Viện Khoa học và Công nghệ Quân sự

[2]Viện Thuốc phóng Thuốc nổ, Tổng cục Công nghiệp Quốc phòng